EE 415 Project Final Report

Osman Melih Muslu
Electrical and Electronics Engineering
Middle East Technical University (METU)
Ankara, Turkey
melih.muslu@metu.edu.tr

***Abstract*—This project explores forward and backprojection techniques in CT imaging, focusing on their implementation and optimization. Forward projection uses the Radon Transform to simulate projection data, while backprojection reconstructs images from these projections. MATLAB-based algorithms allow for adjustable resolutions and filtering methods, including Ram-lak filter and Hamming window, to address common artifacts such as blurring and noise. The results emphasize the critical role of filtering in enhancing image quality and preserving structural details. Additionally, the study highlights the trade-off between computational efficiency and reconstruction accuracy, offering insights into the practical challenges of CT imaging. This work provides a foundation for advancing CT image reconstruction techniques, particularly in developing artifact reduction and noise suppression methods for improved diagnostic imaging.**

Keywords— CT imaging, Radon Transform, forward projection, back projection, MATLAB, filtering, windowing

I. INTRODUCTION

X-ray imaging, discovered by Dr. Wilhelm Roentgen in 1895, marked a transformative moment in medical science. While experimenting with a Crookes tube, Roentgen observed an unknown form of high-energy electromagnetic radiation that could penetrate opaque materials, including human tissue. This accidental discovery enabled the visualization of internal anatomical structures, paving the way for the field of radiology. The first-ever X-ray image, famously depicting the bones in his wife's hand, demonstrated the immense diagnostic potential of this technology, which rapidly gained worldwide attention and clinical application.

Building upon the principles of X-ray imaging, Computed Tomography (CT) emerged in the early 1970s, spearheaded by Sir Godfrey Hounsfield and Allan Cormack. Their groundbreaking work introduced the concept of reconstructing cross-sectional images of the body by combining data from multiple X-ray projections. This advancement addressed the limitations of traditional 2D X-ray imaging, offering a detailed, three-dimensional view of internal structures. Hounsfield and Cormack's contributions were recognized with the Nobel Prize in Medicine in 1979, underscoring the profound impact of CT on medical diagnostics.

Forward projection models the process of acquiring projection data by simulating the interaction of X-rays with the object. Backprojection, on the other hand, uses this data to reconstructed cross-sectional images, enabling clinicians to visualize internal structures with exceptional detail. These methods are critical for achieving accurate and artifact-free reconstructions.

This report explores the motivation behind implementing forward and backprojection algorithms in CT imaging, focusing on their role in reducing artifacts and improving reconstructed image precision. These algorithms are integral to achieving high-quality, accurate visualizations of internal structures, ensuring reliable diagnostics and supporting advanced medical imaging applications.

II. THEORY & ALGORITHM

A. Projection

1) Mathematical Background

The mathematical basis for forward projection lies in the Radon Transform, which integrates the attenuation coefficients of an object along a set of straight paths corresponding to the X-ray beam paths, defined as:

$$p_\theta(t) = \int_{-\infty}^{\infty}\int_{-\infty}^{\infty} f(x,y)\delta(xcos\theta + ysin\theta - t)dxdy \quad (1)$$

Where $p_\theta(t)$ represents the projection at an angle and distance , and δ is the Dirac delta function. The Radon Transform accumulates pixel values along lines defined by the angle and distance .

2) Theoretical Background Steps

a) The process begins by loading the input image into the workspace, typically in .mat format, which efficiently stores the image as a numerical matrix. Each matrix element corresponds to the intensity of a pixel. The dimensions of the image are determined using the MATLAB size function, which provides the number of rows and columns in the image matrix. To ensure the entire image is included in the projection process, the larger of the two dimensions is taken as MMM, defining the spatial extent of the projection grid. This step guarantees that the grid is large enough to accommodate the full image, allowing accurate computations during the projection.

b) Projection angles (θ) and radial distances (t) are essential for forward projection. The angles are defined over the range [0,180], divided into equal intervals using MATLAB's linspace function. The step size of the angles, specified as an input parameter, determines the angular resolution. The t-values, representing the distances of projection lines from the origin, span the range $[-\frac{M}{\sqrt{2}}, \frac{M}{\sqrt{2}}]$, ensuring coverage of the entire image. The number of beams (or sampling points along t) is another input parameter, controlling the radial resolution of the projection.

c) Forward projection involves iterating over the defined θ-angles and t-values using nested loops. The outer loop processes each angle, defining the orientation of the projection lines, while the inner loop iterates through the t-values for that angle, representing different radial distances. This structure ensures that minimal projections are computed for each angle, providing the necessary data for later reconstruction.

d) To compute the projection values, the intersection points of each projection line with the image grid must be determined. The line equation:

$$xcos(\theta) + ysin(\theta) = t \tag{2}$$

is used to calculate the intersection points. For horizontal sweeps, integer x-values within the grid are used to compute corresponding y-coordinates. Similarly, vertical sweeps use integer y-values to find x-coordinates. Only intersection points within the bounds of the image are retained, ensuring that irrelevant points are excluded from further computations.

e) The valid intersection points from horizontal and vertical sweeps are combined into a single matrix and sorted by their x-values. Sorting is crucial for maintaining the order of points along the projection line, facilitating accurate calculations in subsequent steps. Duplicate rows are removed using MATLAB's unique function to prevent redundant computations and improve accuracy.

f) The midpoint and distance between consecutive intersection points are calculated to determine the pixel contributions along the projection line:

$$distance = \sqrt{((x_2 - x_1)^2 + (y_2 - y_1)^2)} \tag{3}$$

$$mid\ points = \frac{x_2+x_1}{2} + \frac{y_2+y_1}{2} \tag{4}$$

The midpoints are mapped to row and column indices in the image grid using:

$$row\_data = \frac{M}{2} - floor(midpoints\_y) \tag{6}$$

$$column\_data = \frac{N}{2} - floor(midpoints\_x) \tag{7}$$

This ensures that the midpoint of each line segment is assigned to the appropriate pixel, enabling accurate accumulation of projection values.

g) Projection values are computed by summing the product of pixel intensities and the distances between consecutive intersection points.

3) Translation into Algorithms

The mathematical background of forward projection, based on the Radon Transform, is translated into implemented algorithms by discretizing the continuous model as seen in [5].

$$p_\theta[i] = \sum_{j,k} f\ [j,k] w_{i,j,k} \tag{5}$$

where $f\ [j,k]$ represents the attenuation coefficient at pixel [j,k] and $w_{i,j,k}$ is a weight factor that represents the contribution of the pixel to the projection ray i. It is often derived using the length of the intersection of the ray with the pixel.

The object is represented as a grid of pixels (2D), and the line integrals are approximated through summations over these discrete elements. In practice, the contribution of each pixel to a specific projection ray is weighted based on the intersection length or area of overlap. For each projection angle, the algorithm rotates the object virtually and iterates over the grid to compute the corresponding projection values, repeating this process for all angles within the specified range. This translation ensures that the theoretical Radon Transform is effectively implemented in a computational framework suitable for generating projection data.

4) Assumptions and Approximations

a) Discrete Sampling

In computational implementations of CT imaging algorithms, continuous integrals, which are central to the mathematical formulations of forward projection, are approximated through discrete summation. This method partitions the continuous domain into finite elements, making numerical computation feasible but inevitably introducing small errors. These discrepancies occur because the discrete grid cannot fully capture the continuous variation of pixel intensities and projection data. Although using higher resolution grids can minimize these errors, it also escalates computational demands, creating a trade-off between achieving greater accuracy and maintaining efficiency.

b) Pixel Approximation

The discrete nature of CT necessitates mapping continuous spatial data to a grid of square pixels. To achieve this, the midpoint of each projection path is used to identify the corresponding pixel within the grid. This is accomplished by calculating the row and column indices of the pixel based on the midpoint coordinates as shown in [6], employing MATLAB's floor and ceil functions.

$$mid\ points = \frac{x_2+x_1}{2} + \frac{y_2+y_1}{2} \tag{6}$$

These functions ensure the approximation of continuous coordinates to the nearest discrete pixel locations. While this is an efficient and practical approach for computational purposes, it may result in slight deviations, particularly when dealing with high-resolution grids or complex structures.

B. *Backprojection*

1) *Mathematical Background*

The mathematical basis for *back*projection lies in the *Inverse* Radon Transform, which involves mapping the projection data collected at various angles back onto the image plane to generate a 2D representation of the object being scanned. The equation [7] shows how back projection reconstructs an image by integrating the projection data $p_\theta(t)$ over all angles from 0 to π and the delta function ensures that the projection value $p_\theta(t)$ contributes only to the (x,y) points lying on the corresponding line in the image space, defined as:

$$f_b(x,y) = \int_0^{\pi} \int_{-\infty}^{\infty} p_\theta(t)\, \delta(x cos\theta + y sin\theta - t) \mathrm{d}t \mathrm{d}\theta \qquad (7)$$

Projection data $p_\theta(t)$ is "smeared" back across the image plane along the lines defined by t and θ. The contributions from all angles are accumulated, giving a rough approximation of the original image f(x,y). Without any filtering, this backprojection creates a blurred image due to the overrepresentation of low-frequency components.

2) *Theoretical Background*

a) The process starts by extracting the dimensions of the projection_data matrix, where num_angles corresponds to the number of projection angles (rows) and num_beams represents the number of sampling points (columns). The reconstruction grid dimensions (r and c) are derived from recons_img_size. The maximum of these dimensions, denoted as M, defines the spatial coverage of the reconstruction grid to ensure the entire image fits within it. The projection angles (theta_values) are evenly distributed between 0° and 180°, while the distance values (t_values) span from $-\frac{M}{\sqrt{2}}$ to $\frac{M}{\sqrt{2}}$, covering the full range of radial projections. For odd num_beams, the center of t_values is shifted to ensure proper alignment of the central projection line with the origin of the reconstruction grid.

b) The reconstruction grid is constructed by defining horizontal and vertical coordinate ranges that extend from −c/2 to c/2 and -r/2 to r/2, respectively. These coordinates establish a spatial domain that serves as the canvas for accumulating contributions from the projection data. To facilitate this, a zero-initialized matrix of dimensions [r,c] is created to act as a neutral baseline, ensuring that the reconstruction process starts without any bias. This matrix will be incrementally updated with projection contributions during the backprojection process. The specified coordinate system provides a structured framework for remapping projection data into the spatial domain, enabling precise alignment of projection contributions with their corresponding locations in the image grid.

c) Blurring in backprojection arises as an intrinsic artifact due to the uneven weighting of spatial frequencies and the cumulative overlapping of contributions from multiple projections. This effect is a result of the backprojection process treating all spatial frequencies equally, without accounting for their differing contributions to the image reconstruction. As projections are mapped back onto the image grid, their overlap creates loss of sharpness and fine details in the reconstructed image, since the reconstructed image lacks the high-frequency components required for sharp details. The backprojected image and the original image have the relation [2] in spatial frequency domain where 1/ ρ term causes to over sampled low frequency components:

$$F_b(\rho,\phi) = F(\rho,\phi)/\rho \qquad (2)$$

Multiplying $F_b(\rho,\phi)\ with\ \rho$ prevents this effect which is an optional filtering step. It is applied to the projection data before backprojection and creates the **filtered backprojection**. The ideal filter to surpress the low frequency components causes blurring is shown in Figure 1.

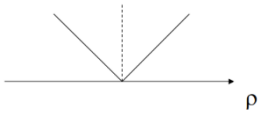

Figure 1: Ideal High Pass Filter

Since it cannot be implemented in the real life, the real life version is a Ram-Lak filter which is the bandlimited version as depicited in Figure 2.

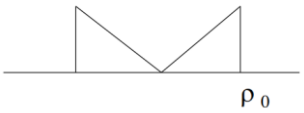

Figure 2: Ram-lak Filter

Since increasing the effect of high frequency components amplifies noise and may introduce ringing artifacts near sharp edges the Ram-lak filter is multiplied by a Hamming window to suppress noise and reduce ringing artifacts caused by sharp transitions in the data.

d) After applying the filtering step, the core backprojection algorithm is executed through nested loops over all projection angles (theta_values) and distances (t_values), following a structure similar to the forward projection process. For each angle, the algorithm determines the intersections of the projection line with the reconstruction grid using geometric relationships. Horizontal sweeps calculate the corresponding vertical coordinates (y_x) for fixed horizontal positions (x), while vertical sweeps compute the horizontal coordinates (x_y) for fixed vertical positions (y). This dual-sweep approach ensures comprehensive coverage of all possible intersections between the projection line and the grid. To maintain accuracy, only valid intersection points—those falling within the bounds of the reconstruction grid—are preserved. For each pair of consecutive intersection points, the distance and midpoint are calculated.These determine the pixel locations in the reconstructed image where the projection contributions are accumulated.

e) The intensity contributions from the projection data are accumulated at the calculated grid indices. For each valid midpoint, the corresponding intensity value from the filtered projection_data is multiplied by the path length and added to the pixel value in the reconstructed_image matrix. This step ensures that the contributions from all projection angles and distances are appropriately distributed across the reconstruction grid. The accumulation process reflects the density of projection data along each line, producing a representation of the original object.

f) Once all projection data has been backprojected, the reconstructed image undergoes normalization to ensure consistent scaling. Each pixel intensity in the reconstructed image can be normalized using one of two methods, depending on the application needs. The first method divides each pixel intensity by the total number of projection angles (num_angles). This type of normalization ensures that the contributions from all projection angles are averaged, providing uniform intensity scaling across reconstructions with varying angular resolutions. The second method normalizes each pixel intensity by the maximum intensity value in the reconstructed image. This approach scales the intensity values so that the highest pixel intensity becomes 1, highlighting relative contrasts within the image. It is ideal for visualization, in our case, as it ensures the image fits well within a grayscale colormap range, enhancing interpretability and aesthetic presentation. Finally, the normalized reconstructed image is displayed using a grayscale colormap, with labeled axes and a colorbar to indicate intensity values.

3) Translation into Algorithms

In backprojection, the continuous integration required to reconstruct an image from its projection data is approximated using discrete summation. This is because digital systems operate on sampled data rather than continuous functions. The mathematical formula for backprojection involves integrating the projection data $p_\theta(t)$ over all angles θ and distances t, but in practice, this is replaced by a summation over a finite number of angles and discrete spatial positions.

$$f_b[x, y] = \sum_{\theta, t} p_\theta(t)\, w_{x,y,\theta,t} \qquad (8)$$

Where $w_{x,y,\theta,t}$ represents the interpolation weights to distribute the projection data over the discrete grid. This summation process involves calculating contributions from projection data at specific angles and redistributing them across the pixels in the reconstructed grid.

4) Assumptions and Approximations

a) Discrete Sampling

Discrete sampling errors in backprojection arise because continuous projection data, which is theoretically integrated over infinite angles and spatial positions, must be approximated using a finite number of discrete samples. These errors are a direct consequence of the finite angular resolution and spatial sampling intervals used in computational implementations. In backprojection, the angular range [0,180] is divided into a finite number of angles, and projection data at discrete distances (t-values) is mapped back onto the image grid. If the sampling resolution is too low, critical details of the image can be missed, leading to artifacts such as streaking or blurring in the reconstructed image. Additionally, when the projection lines do not perfectly align with the discrete grid of pixels, interpolation or approximations (floor,ceil etc.) are required, which can introduce further inaccuracies. These errors can be mitigated by increasing the number of projection angles or using finer spatial sampling, but this comes at the cost of higher computational requirements. Thus, discrete sampling errors highlight the inherent trade-off between accuracy and computational efficiency in backprojection algorithms.

b) Image Boundries

CT imaging relies on projecting and reconstructing data within a defined spatial domain. Projections that extend beyond the image boundaries are typically ignored in the implementation of forward and backprojection algorithms. This limitation simplifies computations but may omit contributions from parts of the projection data, particularly when dealing with objects that extend beyond the defined reconstruction grid. As a result, the reconstructed image might lack information at the edges, potentially leading to inaccuracies or truncation artifacts.

c) Filter Design

The use of a frequency-domain filter, such as Ram-lak, is essential for reducing artifacts in backprojection. However, practical implementations rely on approximations of ideal high-pass filters due to physical and computational limitations. The comparison of ideal and practical Ram-lak filter is shown in Figure 1.

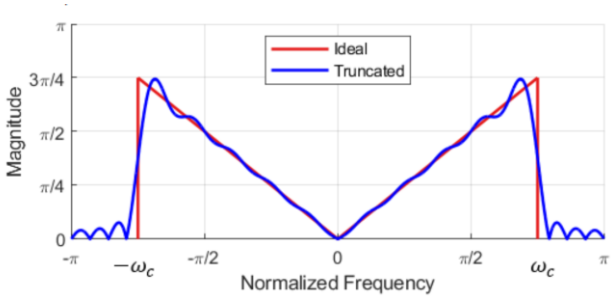

Figure 1: Ideal (red) and real (blue)Ram-lak Filter.

The ideal Ram-lak filter (red) features a sharp frequency cutoff, allowing high-frequency components to pass through without attenuation, which preserves edge details and enhances sharpness in the reconstructed image. However, this sharp transition also amplifies noise, particularly in high-frequency regions, and may introduce ringing artifacts near sharp edges (Gibbs phenomenon). On the other hand, the practical Ram-lak filter (blue) smooths the frequency response with a gradual transition at the cutoff, effectively suppressing noise and reducing artifacts.

While this modification enhances the filter's robustness in noisy environments, it slightly compromises edge clarity and detail preservation. Overall, the ideal Ram-lak filter is suited

for applications prioritizing sharpness, while the windowed Ram-lak filter offers a balanced approach for noisy or artifact-prone datasets.

Ideal filters theoretically resolve low-frequency oversampling issues with precision, their implementation is infeasible as they demand infinite resolution and precision. As a result, real-world filters are optimized to balance artifact reduction and noise suppression. Despite these optimizations, they cannot completely eliminate artifacts, leaving subtle distortions in the reconstructed images.

III. RESULTS & DISCUSSION

A. *Projection*

1) *General Comment*

a) Simple Image

The results of the forward projection for a square image were successfully computed. The image was selected for its simplicity, allowing for a clear demonstration of how projections are computed across various angles. The projections were generated at several angles ranging from 0° to 180°, with a specified step size. As expected, the projections at different angles exhibit variations based on the structural features of the image. For each angle θ, the projection values represent the accumulated pixel intensity along the corresponding projection lines at various distances t from the center of the image.

The projections at smaller angles (e.g., near 0° or 180°) capture more information about the horizontal features of the image, while projections at angles near 90° capture more about the vertical features. As can bee seen from the Figure 2, the projections of 0° and 90° are rectangle-shaped whereas in the projections of 45° and 135° it is triangular-shaped. This due to the shape of a square, which results in projections will capture the maximum intensity because the projection lines cut across the full width of the square. This typically leads to the highest peaks in the projection profiles for these angles.

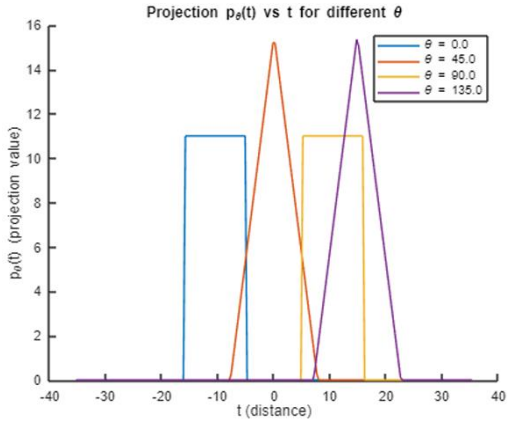

Figure 2: Projections for Different Angles of a Square.

b) Complex Image

When the input image is more complex or contains irregular shapes—the projections at different angles reveal more detailed information about the structure of the image. These projections will be influenced not only by the geometry of the image but also by the distribution of pixel intensities and unlike a simple square image, a complex image can have multiple regions with different characteristics. For example, it could contain edges, curves, or noisy textures. These factors significantly impact the projection profiles. The choosen complex image is Lena shown in Figure 3.

Figure 3: The Complex Image 'Lena'.

As can be seen from the 0° projection result of Lena in Figure 4, we see two different pehaks at projection values due to the high contrasts in those vertical lines. One of them corresponds to the white wood on the left, while the other corresponds to the tip of Lena's nose.

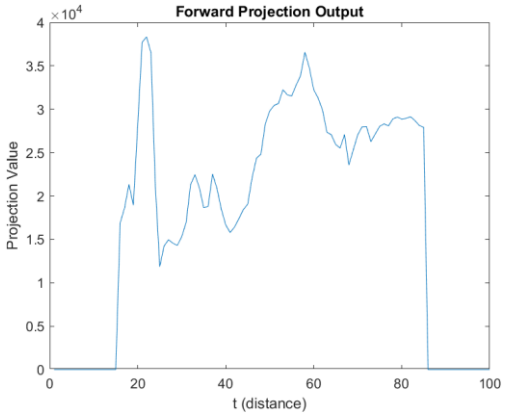

Figure 4: The 0° Projection of Lena.

2) *Hand Calculated Results*

For an arbitrary image, projection formula is given below for a specific angle:

$$p_\theta[t] = \sum_{\substack{-15\le x\le -5 \\ 5\le y\le 15}} f[x,y] * \delta(x\cos\theta + y\sin\theta - t)dxdy \quad (9)$$

If we simplify for a 0° Projection, equation becomes:

$$p_0[t] = \sum_{\substack{-15\le x\le -5 \\ 5\le y\le 15}} f[x,y] * \delta(x\cos 0 + y\sin 0 - t)dxdy \quad (10)$$

where $f[x,y] = 1$.

As the equation proceeds:

$$p_0[t] = \sum_{-15\le x\le -5} \delta(x - t)dx \quad (11)$$

The final result becomes:

$$p_0[t] = 11$$

Which can be seen in a $0°$ Projection value in Figure 5.

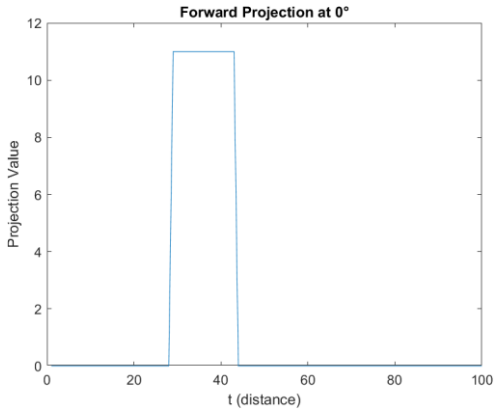

Figure 5: The $0°$ Projection of Square.

B.Backprojection

1) Image Complexity

The backprojection process behaves differently when reconstructing simple versus complex images due to variations in spatial frequency content and structural complexity. Simple images, such as geometric shapes like squares or circles, are characterized by uniform intensity regions and distinct edges. In comparison, complex images, which feature a combination of high-frequency elements (such as edges and fine textures) and low-frequency elements (such as smooth gradients), pose greater challenges for backprojection. The backprojection comparison of simple and complex images is depicited in Figure 6a and 6b:

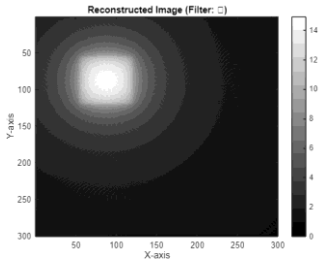

Figure 6a: Backprojection of a Square.

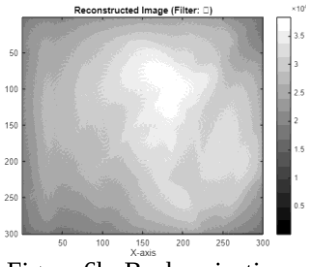

Figure 6b: Backprojection of Lena.

Several inferences be made from Figure 6a and 6b.

- In the simple image, during backprojection the contributions from projection lines are evenly distributed, and the reconstructed image typically exhibits sharp edges. However, due to the inherent limitations of unfiltered backprojection, slight blurring or streaking artifacts may still be observed, especially at high-contrast boundaries.
- In the complex image, Non-filtered backprojection tends to blur fine details and can amplify overlapping contributions, resulting in smeared textures. Despite this, the overall structure of the image is preserved, albeit less sharply than with filtered backprojection.

Hence, the backprojection of complex images is more sensitive to noise and resolution, as much more high-frequency components may be underrepresented or distorted.

2) Projection Data Specifications

Also, The **number of projections** and **projection angles** in the forward projection directly affects the quality of the reconstructed image by determining the completeness of the angular and radial coverage.

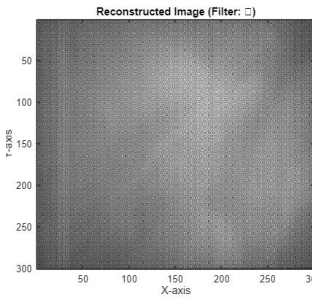

Figure 7a: B.P of Lena at 10 degree step size and 250 beams.

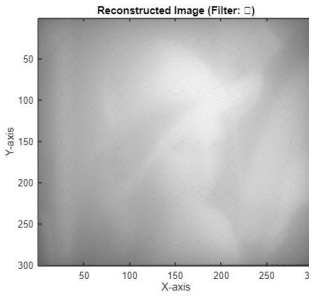

Figure 7b: B.P of Lena at 1 degree step size and 400 beams.

As can be seen from Figure 7a and 7b, with more beams, the projection data are densely sampled, capturing finer details and improving the radial resolution and with more projections, the contributions from overlapping projection lines blend smoothly, reducing streaking artifacts and enhancing the overall clarity of the image. But since we haven't applied any filters yet, blurring is still there. Increasing both parameters leads to diminishing returns beyond a certain point, as excessively fine angular and radial resolutions may not significantly improve image quality but will increase computational cost. An optimal balance must be found.

The filter is essential for addressing the blurring artifacts inherent in the backprojection process, as it compensates for the uneven weighting of spatial frequencies. We selected the Ram-lak filter since its linear ramp-like frequency response emphasizes high-frequency components, allowing fine details and sharp edges in the reconstructed image to be accurately preserved. Without the application of the Ram-Lak filter, the reconstructed image would be dominated by low-frequency components, resulting in overly smoothed visuals with indistinct and blurred boundaries as depicited in Figure 8a.

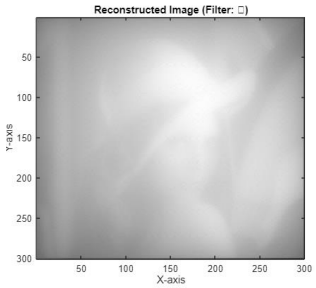

Figure 8a: Backprojection of Lena.

Figure 8b: Filtered Backprojection of Lena.

As shown in Figure 8b, when we applied Ram-lak filter, it significantly improves edge sharpness and restores fine details, making the reconstructed image more accurate.

3) Quantitative Demonstration

The Mean Squared Error (MSE) values provide a quantitative measure of the reconstruction accuracy for backprojection and filtered backprojection methods. The significantly higher MSE for the backprojection without filtering (3.9606×10^-2) compared to the filtered backprojection (1.4517×10^−3) highlights the impact of filtering on improving image quality. In the case of unfiltered backprojection, the reconstruction process treats all frequency components equally, resulting in the oversampling of low-frequency components. This leads to blurring in the reconstructed image, as low-frequency dominance suppresses high-frequency details critical for edge sharpness and fine structures. Consequently, this blurring is reflected in the higher MSE, which indicates a greater deviation from the original image.

Filtered backprojection mitigates this issue by applying a high-pass filter, such as the Ramp filter, in the frequency domain. This filter amplifies the high-frequency components while attenuating the overrepresented low frequencies, restoring edge sharpness and enhancing the overall image detail. The reduced MSE (1.4517×10^−3) demonstrates the effectiveness of this approach in reducing artifacts and improving the fidelity of the reconstructed image. Additionally, combining the Ramp filter with a windowing function, such as a Hamming window, can suppress ringing artifacts caused by sharp transitions in the frequency response, further improving the reconstruction quality.

C.Filtered Backprojection

The high-frequency emphasis of the Ram-Lak filter, while effective at preserving fine details and sharp edges, can also amplify noise, especially in areas with high contrast or where measurement inaccuracies are present. Windowing introduces a smooth transition in the filter's response, effectively balancing sharpness and noise suppression. While this results in slightly less edge enhancement compared to the unmodified Ram-Lak filter, it produces reconstructions that are smoother and less prone to artifacts as shown in Figure 6a and 6b.

Figure 9a: Filtered Backprojection of Lena.

Figure 9b: Windowing Filtered Backprojection of Lena.

To conclude, the combination of the Ram-Lak filter with the Hamming window is particularly advantageous for noisy projection data of complex images.

1) Quantative Demonstration

When windowing is applied in filtered backprojection, the Mean Squared Error (MSE= 2.5507×10^−3) increases slightly compared to using a pure Ramp filter without a window. This is because windowing modifies the frequency response of the filter, trading off some sharpness in high-frequency components to reduce noise and ringing artifacts. In the frequency domain, the Ramp filter amplifies high-frequency components, which are crucial for capturing edge details and fine structures. However, this high-frequency emphasis also amplifies noise, particularly in regions where the data is sparse or corrupted, leading to potential artifacts.

Windowing functions, such as the Hamming or Hann window, smooth the frequency response of the Ramp filter by tapering the high-frequency components. This smooth transition reduces noise amplification and mitigates ringing artifacts caused by abrupt changes in the filter response. However, by attenuating high frequencies, windowing also suppresses some of the high-frequency details in the reconstructed image, which can cause the reconstructed image to deviate slightly from the original. This trade-off results in an increase in MSE, as the reconstruction no longer fully preserves fine details due to the reduced contribution of high-frequency information.

IV. CONCLUSION

This project comprehensively explored the forward and backprojection techniques central to CT imaging, addressing their theoretical foundations, implementation, and practical implications. The forward projection method was developed to simulate the generation of projection data using the Radon Transform, while the backprojection technique reconstructed images from these projections. Through detailed MATLAB implementations, we successfully demonstrated the interplay between computational efficiency, parameter tuning, and reconstruction accuracy. One critical achievement was the validation of the forward projection function using a simple image with analytically available projections. The consistency between hand-calculated and simulated results affirmed the reliability of the implementation. For complex

images, the forward projection demonstrated its ability to capture intricate structural details, though minor artifacts such as streaking were observed.
The backprojection method, implemented with and without filtering, further illuminated the challenges and trade-offs in CT image reconstruction. The unfiltered backprojection produced blurred reconstructions due to the dominance of low-frequency components. Filtering effectively compensated for the oversampling of low frequencies, restoring the balance in the frequency domain and improving the visual quality of the reconstructed images.

However, the application of windowing functions, such as the Hamming window, introduced a nuanced trade-off. While these functions reduced noise amplification and ringing artifacts, they also attenuated high-frequency details, leading to a slight increase in MSE. This underscores the delicate balance between noise suppression and detail retention, which is fundamental to the design of CT reconstruction algorithms.

Another vital aspect was the sensitivity of both forward and backprojection techniques to parameter selection. Factors such as angular step size, beam spacing, and the size of the reconstruction grid significantly influenced the quality of projections and reconstructions. Smaller step sizes and finer beam resolutions improved accuracy but increased computational demands, emphasizing the trade-off between precision and efficiency. Moreover, the use of discrete sampling and numerical approximations, while practical for digital implementations, introduced minor inaccuracies that require careful management through parameter optimization.

This project highlights the importance of filtering in mitigating artifacts, the role of parameter tuning in optimizing reconstruction quality, and the inherent trade-offs in computational imaging. While the implemented methods demonstrated robust performance, they also revealed the limitations and challenges of practical CT imaging, such as noise sensitivity and approximation errors. These findings provide a strong foundation for further exploration of advanced reconstruction techniques, such as iterative methods and machine learning approaches, which could enhance the accuracy and efficiency of CT imaging.

In conclusion, the project successfully achieved its objectives by developing and analyzing forward and backprojection methods, offering valuable insights into their theoretical underpinnings, practical implementation, and critical performance factors. The results not only validate the effectiveness of these techniques but also emphasize the need for ongoing innovation in CT image reconstruction to address the challenges of modern medical imaging.

V. REFERENCES

[1] "X-ray Information," Sunnybrook Research Institute. Accessed: Dec. 30, 2024.[Online].Available: https://sunnybrook.ca/research/content/?page=sri-groups-xray-info-3

[2] The Nobel Prize in Physiology or Medicine 1979," NobelPrize.org. [Online].Available: https://www.nobelprize.org/prizes/medicine/1979/summary/

[3] Q. Zhang, "Design of a discrete-time differentiator," Wireless Pi. Accessed: Dec. 30, 2024. [Online]. Available: https://wirelesspi.com/design-of-a-discrete-time-differentiator/